Influence of Monomer Deformation on the Competition Between Two Types of σ-Holes in Tetrel Bonds

Rafał Wysokiński,*[1] Mariusz Michalczyk,[1] Wiktor Zierkiewicz[1] and Steve Scheiner*[2]

[1]Faculty of Chemistry, Wrocław University of Science and Technology, Wybrzeże Wyspiańskiego 27, 50-370 Wrocław, Poland

[2] Department of Chemistry and Biochemistry, Utah State University, Logan, Utah 84322-0300, United States

Abstract

One of several tetrel (T) atoms was covalently attached to three F atoms and a substituted phenyl ring. A NH_3 base can form a tetrel bond with $TF_3C_6H_2R_3$ (T = Si, Ge, Sn, Pb; R = H, F, CH_3) in a position opposite either an F atom or the ring. The σ-hole opposite the highly electron-withdrawing F (T-F) is more intense than that opposite the ring (T-C). However, when the Lewis base deforms from a tetrahedral to a trigonal bipyramidal shape so as to accommodate the base, it is the T-C σ-hole that is more intense. Accordingly, it is the T-C tetrel-bonded complex for which there is a larger interaction energy with NH_3, as high as 34 kcal/mol. Countering this trend, it requires more energy for the $TF_3C_6H_2R_3$ to deform into the geometry it adopts within the T-C complex than within its T-F counterpart. There is consequently a balance between the overall binding energies of the two competing sites. The smaller tetrel atoms Si and Ge, with their larger deformation energies, show a preference for T-F tetrel binding, while the T-C site is preferred by Pb which suffers from a smaller degree of deformation energy. There is a near balance for T=Sn and the two sites show comparable binding energies.

Keywords: σ-hole, deformation energy; MP2; MEP; AIM

*Correspondence to: rafal.wysokinski@pwr.edu.pl, steve.scheiner@usu.edu

1. INTRODUCTION

Noncovalent interactions drive an entire range of chemical and physical phenomena, such as self-assembly, intermediate products of organic synthesis, and stabilization of crystal structures.[1-9] Their role is also undisputed in biochemical processes[10-12], for example underpinning the connections between receptors and ligands which facilitate protein transport, or enzymatic catalysis.[13-18] A thorough understanding of the fundamental nature of noncovalent interactions and their role in controlling molecular complexes is one of the linchpins for future progress of modern chemistry.

The concept of the σ-hole[19-23], introduced with a view toward clarifying halogen bonding phenomenon[23-31] has been extended to a large family of noncovalent interactions where an electronegative atom is able to interact with a nucleophile. Although at first glance implausible, the attractive force is based on a local depletion of electron density around the halogen[32, 33], chalcogen[34, 35], pnicogen[36, 37], tetrel[38-40] or noble gas atoms[41-44], usually directly opposite a σ-bond, hence its common appellation as a σ-hole.[45] Study over the years[46-49] has established that the strength of each σ-hole is enhanced by reduced electronegativity and enhanced polarizability of the central atom, coupled with electron-withdrawing power of its substituent.[23, 47-51] On the other side of the equation, the interaction will be strengthened by a more powerful nucleophile.[25]

Given these basic rules it ought to be possible to tune the σ-hole noncovalent bond to any desired strength, by appropriate modification of central atom or substituent. And indeed, there have been numerous studies that demonstrated this principle.[52-58] In one example, Riley *et al.*[56-58] demonstrated that substitution of heavier central halogens leads to a larger σ-hole and consequently to a stronger interaction, more electrostatic in nature. Politzer and Murray[25] presented, in turn, a correlation between σ-hole intensity and interaction energies for 18 halogen bonded complexes with NCH.

However, the situation is not quite so simple. Firstly, the interaction is not wholly electrostatic. Charge transfer makes a major contribution as well, augmented by dispersion forces.[37, 39, 59-64] There are also other factors that mitigate against a strict correlation between interaction energy and σ-hole intensity.[65-69] There are geometric deformations that accompany complexation[65] that influence both the σ-hole depth and the overall energetics. Negative hyperconjugation may alter the electron-donating potential of the Lewis base,[68] and spin density in open-shell coinage metal clusters[66] may significantly perturb the correlation between σ-hole and complex stability. It is clear then that more detailed study of these and other effects is required before reaching a full understanding of this phenomenon.

Tetrel bonds, described as "the tendency of heavier tetrel atoms to interact with anions or electron rich atoms"[70] belong to this family of σ-hole bonds, and have benefited from recent study, both theoretically and experimentally.[71-79] As a very recent example, calculations of the TH_3^+ (T = C, Si, Ge) complexes with H_2 showed that H_2 can serve as a tetrel bond acceptor through its σ-bond, and that the fundamental nature of the TH_5^+ depends on the identity of the T atom. It has also recently been reported that an S···Sn contact plays a crucial role in activation of peroxisome proliferator-activated receptors (PPARs) by organotin molecules.[80]

While the relationship between electron-withdrawing power of a substituent and the intensity of the σ-hole which it causes is fairly straightforward at this point, there are numerous indications that the σ-hole is not the only arbiter of the strength of the noncovalent bond. This lack of clarity is particularly at issue for tetrel bonds for a number of reasons. In the first place, the presence of four surrounding substituents around a tetrel atom leads to an obstructed path for an approaching nucleophile so the molecule must therefore deform a good deal so as to make the necessary room. The resulting deformation energy must be overcome in order for a stable tetrel bond to be formed. The deformation also changes both the qualitative and quantitative character of the σ-holes relative to the undistorted monomer. These holes not only alter their intensity but can even change from σ to π in nature.

The work presented here aims to develop a more thorough and sophisticated means of understanding the competition between possible tetrel bonding sites on a given molecule. The intensities of the σ-holes, and how they are affected by each particular substituent, are taken as a starting point in this competition. The interaction of a nucleophile with each site is then elucidated, using various measures including, energetic, geometrical, and those derived from the wave functions. As another important consideration, the structural deformation undergone in order to facilitate the tetrel bond formation is considered, and how this transformation affects both the electrostatic potential and the energetics of the system. The results demonstrate how important these geometric deformations are, and how they can affect the competition between the possible tetrel bond sites, even reversing the expected trends.

2. SYSTEMS AND METHODS

In order to facilitate this comparative study, the Lewis acid was composed of a single tetrel atom, covalently bonded to three F substituents and one phenyl ring. The latter was considered as a simple C_6H_5, but also with two sorts of substituents. F atoms are known to be strongly electron-withdrawing, whereas methyl groups act in the opposite fashion. Whether F or CH_3, three such substituents were placed on the phenyl ring to maximize their activity. They were placed para to the connection to the tetrel atom, and in both meta locations. Avoidance of ortho positions reduced the possibility of interactions with the F substituents on the tetrel atom which would complicate the analysis. The entire range of tetrel atoms from C to Pb were considered as the central atom so as to elucidate how its nature affects the properties of the interactions. In sum, the Lewis acids are denoted $TF_3C_6H_2R_3$ where T refers to the tetrel atom and R to either H, F or CH_3. The Lewis base chosen as NH_3, due to its strong nucleophilic nature, and its simplicity which will again minimize secondary interactions.

The geometries of isolated $TF_3C_6H_2R_3$ molecules and their binary complexes with NH_3 were optimized at the MP2 level of theory with the aug-cc-pVDZ basis set.[81, 82] For the heavy Sn and Pb atoms pseudopotentials were used which include some relativistic effects.[83] The absence of an imaginary frequency guaranteed that the structures are true minima. Additionally, calculations at the BLYP-D3/aug-cc-pVDZ[81, 84, 85] level of theory were performed for complexes so as to obtain DFT geometries and energetics with which the MP2 quantities can be compared. The

CCSD(T)/aug-cc-pVDZ[86] level, using MP2 optimized minima, was also employed in order to further validate the energetics,. Interaction energies E_{int} take as their reference the energies of the monomers in the internal geometries they adopt within the complex. Binding energies E_b were evaluated with respect to separately optimized monomers. These two quantities thus differ by the deformation energies required to distort the monomers from their isolated geometry to that adopted in the complex. Both interaction and binding energies were corrected for basis set superposition error via the standard counterpoise procedure.[87]

The MultiWFN[88, 89] and WFA-SAS[90] programs were used to compute and visualize the molecular electrostatic potential of isolated monomers. Aspects of the bonding were analyzed via a topological analysis of the electron density using AIMAll[91] software based on the MP2 wave function. The NBO method (GenNBO 6.0 software)[92] was applied to measure orbital-orbital interactions and charge transfer between interacting subunits. The EDA energy dissection embedded in ADF software was executed at the BLYP-D3/ZORA/TZ2P level to compare the various components of the full interaction energy.[93-95] Finally, a CSD (Cambridge Structural Database, CCDC 2019, ConQuest ver. 2.0.1)[96] survey was performed to search for experimental evidence of the bonding scenarios considered in this work. Geometry optimizations and energetics were computed via the Gaussian09 suite of programs.[97]

3. RESULTS

3.1. Monomer Properties

The isolated $TF_3C_6H_2R_3$ (T = C, Si, Ge, Sn, Pb; R = H, F, CH_3) monomers were fully optimized with no symmetry constraints. The phenyl ring and three fluorine atoms are disposed in a tetrahedral arrangement around the tetrel atom, as displayed in Fig. 1. There is a slight difference between the structures for the heavy and light tetrel atoms. For T = Sn, Pb one of the F atoms of the TF_3 group is coplanar with the aromatic ring (Fig 1C) while it lies perpendicular to the aromatic plane for Si and Ge (Fig 1B). This distinction is present at both MP2 and BLYP-D3 levels.

The molecular electrostatic potential (MEP) of $GeF_3C_6H_2R_3$ is illustrated in Figure 2 for R=H, F, and Me as representative of all of the tetrel atoms. Blue negative areas encircle the F atoms while there are red positive regions (so-called σ-holes) lying opposite each T-F bond, as well as opposite the T-C bond involving the phenyl ring. The values of the MEP maximum on the 0.001 au isodensity surface ($V_{s,max}$) for each of these holes are listed in Table 1. There are a number of trends that are worth stressing. In the first place, $V_{s,max}$ grows as the T atom enlarges C<<Si<Ge<Sn~Pb. These holes are especially weak for T=C, which accounts for the failure of $CF_3C_6H_2R_3$ to engage in tetrel bonds with the NH_3 base. As a second issue, regardless of the nature of the tetrel atom, or of the substituents on the aromatic ring, $V_{s,max}$ is consistently larger for the holes opposite the F atoms (T-F hole) than for the corresponding T-C hole opposite the aromatic ring. Also of note, the difference between these two hole types increases as the T atom enlarges. More specifically, this difference is about 7, 15, 21, 36 kcal/mol for the respective Si <Ge <Sn <Pb series. The nature of the R substituent has little bearing on this difference, but it does influence the intensity of the σ-holes, which follows the pattern CH_3 < H < F. This order conforms to

conventional ideas about an electron-withdrawing substituent enlarging the related σ-hole. In quantitative terms, the replacement of H by F enlarges $V_{s,max}$ by 8-11 kcal/mol, whereas the H→Me substitution reduces the intensity by 4-7 kcal/mol.

3.2. Complexes

3.2.1. Equilibrium Geometries and Energies

Given the finding of both T-F and T-C σ-holes, it is not surprising to find that the NH_3 base can interact with either of these two hole types in a tetrel bond. Two different views of each of these two tetrel bond types are illustrated in Fig 3. The two structures are of comparable energy, within some 4 kcal/mol or less of each other. Table 2 reports this energy difference (E_{ele}) at each of two different levels of theory; the values in parentheses represent the free energy differences (G) at 25 C. Positive values indicate a greater stability for the T-F complex. In other words, T-F structures are energetically preferred for the lighter tetrel atoms, whereas the balance shifts toward T-C for Sn and Pb. Note that this competition between the two structures is essentially the same, even quantitatively, whether it is E_{ele} or G that is considered, nor is this result sensitive to the level of theory. The greater stability of the T-C structures for Sn and Pb is perhaps surprising in light of the more intense T-F σ-holes reported in Table 1. Indeed, the T-F values of $V_{s,max}$ are several times larger than their T-C analogues for T=Pb.

The values of the binding energies, representing the difference in energy between the complex and the reactant monomers in their optimized geometries, including counterpoise corrections, are listed in Table 3. Note that there is remarkable agreement amongst all three levels of theory, whether MP2, BLYP-D3, or CCSD(T). These quantities rise in the order Si < Ge < Sn ~ Pb. They are smallest for the T-C complexes for T=Si, as small as -1 kcal/mol for $SiF_3C_6H_2(CH_3)_3$, and grow to a maximum of as much as -20 kcal/mol for $SnF_3C_6H_2F_3$ and $PbF_3C_6H_2F_3$. Again, one sees the pattern that the T-C complexes of the heavier T atoms have a more exothermic binding energy than their T-F structures, despite the opposite trend in $V_{s,max}$.

Some clues to this curious behavior can be gleaned from the structural parameters contained in Table 4. In the first place, the intermolecular R(T⋯N) distance tends to be shorter for the T-C complexes. This difference is roughly 0.08 Å for T=Si, rises to 0.10 Å for Ge and Sn, but then increases above 0.20 Å for Pb. So one can surmise that the stronger T-C tetrel bonds for the heavier T atoms are associated with their shorter nature. An optimal tetrel bond will typically have a linear arrangement between the base and the substituent which it lies opposite to. The θ(X-T⋯N) angles in Table 4 are all in the general vicinity of 180°. However, their variance from this optimal angle increases as T becomes larger. Also, the θ(C-T⋯N) angles are more linear than their θ(F-T⋯N) counterparts. This greater linearity represents a second factor which shifts the energetic preference toward the T-C complexes.

A third factor has to do with the geometry surrounding the T atom. The addition of a fifth ligand to an already tetrahedrally substituted central T involves displacement of the substituents so as to make room for the incoming base. If one thinks of the three T-F bonds as the spokes of an umbrella, then placement of the NH_3 opposite one of these T-F bonds will tend to partially

"close" the umbrella as the F atoms come closer together as in Fig 3A. The opposite effect of a more open umbrella will be the result of a base approaching opposite the C atom in Fig 3B. These effects are summarized by the Σθ(F-T-F) columns in Table 4. Taking $SiF_3C_6H_5$ in the first row of Table 4 as an example, the sum of the three θ(F-T-F) angles is 310° in the T-F complex. This quantity is 10.7° less than in the uncomplexed monomer, representing a partial closure of the umbrella. Formation of the T-C complex, in contrast, forces the umbrella open so that the sum of the three angles is 352.9°, some 32.2° larger than in the monomer. And indeed, the changes in the angle sum is much larger for the T-C than for the T-F complexes for all systems examined here. Whereas this quantity diminishes by some 10-12° for the various T-F structures, it increases by 31-42° for T-C, especially large for Pb.

An alternate way to look at this situation is as follows. In an idealized fully tetrahedral situation of the uncomplexed monomer the angle sum would be 3x109.5° = 329° . A similarly idealized structure of the complex with its five substituents would be trigonal bipyramidal. If the NH_3 takes an axial position directly opposite the phenyl ring, the three F atoms would all occupy equatorial positions, 120° from one another, for a Σθ(F-T-F) sum of 360°. It is for this reason that the quantities in the last column of Table 4 approach this value, and represent a sizable increase over the much smaller sum in the monomer. In the T-F complexes, the axial positions of the trigonal bipyramid are occupied by NH_3 and one of the F atoms, leaving the two remaining F atoms in equatorial sites. The Σθ(F-T-F) sum in this idealized configuration would be 2 x 90° + 120° = 300°, smaller than the 329° in the monomer. This behavior accounts for the decreases observed in the angle sum for the T-F complexes in Table 4.

One last issue has to do with the particular position and orientation of the NH_3 molecule within the T-F complexes. For T=Sn and, Pb, the N lies in the aromatic plane, i.e. φ(C-C-T⋯N) = 0. It is lifted above this plane by some 30° for Ge, and up to 60° for Si. With respect to the rotation of the NH_3 around the N⋯T axis, one of the NH bonds is eclipsed by a T-F bond for $PbF_3C_6H_5$ and $SnF_3C_6H_5$ complexes, whereas these bonds are staggered in the other complexes.

As mentioned above, there is a good deal of angular deformation that accompanies tetrel bond formation, particularly in the T-C complexes. The energetic consequences are contained in Table 5 which reports the deformation energy of both the Lewis acid and base for each dimer. There is very little deformation of the NH_3, amounting to less than 0.2 kcal/mol. But the geometry changes imposed on the Lewis acid result in large energy increases. These deformation energies are largest for the smallest tetrel atoms: Si > Ge > Sn > Pb. With respect first to the T-F complexes, E_{def} varies from 15 kcal/mol for $SiF_3C_6H_2F_3$ down to only 3 kcal/mol for the Pb acids. But consistent with the larger angular changes in the T-C structures, their deformation energies are correspondingly larger. E_{def} ranges from 23 kcal/mol for T=Si down to 12 kcal/mol for Pb, still rather large.

One can view the larger deformation energies in the T-C complexes through the lens of the idealized trigonal bipyramidal geometry. According to standard VSEPR ideas, equatorial sites suffer from less steric repulsion from the other substituents than do axial positions. As a larger

and bulkier substituent, the phenyl ring would naturally be favored for an equatorial location over F. The T-C conformation forces the phenyl ring into the more crowded axial position which is accompanied by a larger deformation energy, as compared to an equatorial position for the phenyl ring in the T-F geometry.

E_{int} refers to the interaction energy between pre-deformed monomers, so can perhaps be thought of as a pure measure of the interaction within the complex. The values of E_{int} in Table 6 are all more negative than E_b following subtraction of the deformation energies. An initial inspection of the data shows that MP2 and CCSD(T) quantities are quite similar to one another, with BLYP-D3 values a bit less negative. Nonetheless, all levels of theory display the same trends. T-C interaction energies are consistently more negative than their T-F counterparts. This difference lies in the 6-8 kcal/mol range, except for T=Pb where the difference enlarges to 12 kcal/mol. This pattern is somewhat different than the E_b trends in Table 3 where the T-F complexes were preferred for the smaller T atoms. This distinction rests on the very large deformation energies of the T-C complexes for the smaller tetrel atoms, which act to disfavor these structures. In terms of their magnitudes, the interaction energies climb consistently from Si to Ge to Sn, but then fall in the transition from Sn to Pb. Indeed, the interaction energies of the Pb T-F dimers are less exothermic than those for Si. Whereas some of the binding energies were quite small, particularly for the small T atoms, the interaction energies are considerably more exothermic. As an example of the strong role played by the deformation energies, the interaction energies for the T-C Si complexes all exceed -20 kcal/mol. In contrast, E_b for these same structures are -5 kcal/mol or even less.

There is a secondary issue with respect to the deformation of the Lewis acid monomer upon complexation with the base. The transformation from a basically tetrahedral structure into a modified trigonal bipyramid amplifies the magnitude of the σ-hole. The last column of Table 5 displays the value of $V_{s,max}$ within the context of the modified monomer, followed in parentheses by its increase relative the optimized tetrahedral monomer. These increases are quite large, and will aid in the formation of the complex by better attracting the nucleophilic base. With regard first to the T-F σ-holes, the increases are in the 30-40 kcal/mol range for Si and Ge, then decrease steadily for Sn and then for Pb. The hole magnifications are even larger for the T-C geometries, in the general range of 50-70 kcal/mol. So while the σ-holes are more intense for T-F than for T-C in the undistorted monomers (Table 1), the reverse is true once the monomers attain the geometry within each complex. It might be concluded then that this larger magnification of the T-C σ-holes is one factor in their larger interaction energies.

3.2.2 Analysis of Wave Function

The AIM analysis technique[98, 99] provides a window into molecular interactions that focuses exclusively on the electron density rather than energetics. The bond paths between nuclei are presented in Fig S1 and the important properties of the intermolecular bond critical point in each complex are contained in Table 7. The AIM data in Table 7 are consistently larger for T-C than for T-F complexes, consistent with the interaction energies in Table 7. AIM also reproduces the

stronger binding of the trifluorosubstituted phenyl rings. On the other hand, AIM mimics certain aspects of the interaction energies with regard to the identity of the T atom. In the case of the T-F complexes, AIM correctly predicts the near equivalence between Si and Pb, but places Ge on a par with Sn although the latter has larger E_{int}. The AIM order for T-C complexes is Si < Ge ~ Sn < Pb while the interaction energies are larger for Sn than for Ge, with Pb roughly equivalent to Sn. Table S1 reports properties of any secondary intermolecular interactions that were suggested by AIM molecular diagrams. These are rather small when they occur at all. For example, the values of ρ at secondary bond critical points are generally about 0.010 a.u., as compared to the same quantities at the primary T⋯N critical point that are five to eight times larger.

NBO offers a means of examining aspects of the charge transfer between the two monomers. Table 8 lists the selected values of the second order interaction energy (E2) between the NH_3 N - lone pair and various orbitals of the Lewis acid. Most of this transfer occurs into what NBO deems a vacant lone pair orbital of the tetrel atom, designated LV*(T). There is also a smaller amount that is transferred to the σ*(T-C) antibonding orbital. The patterns in Table 8 are quite clear. The interorbital interaction is considerably larger for the T-C as compared to the T-F complexes, by nearly a factor of 2. One also sees a clear lowering of this quantity as the T atom grows larger. The CT columns of Table 8 report the total charge transferred from base to acid, regardless of orbital. This measure reinforces the interorbital idea of larger charge transfer for T-C vs T-F. It also shows an increasing Si < Ge < Sn < Pb trend, but only for the T-C complexes. The T-F structures show their largest values for Ge and Sn, followed by Si and with the smallest amount for Pb. It was wondered whether some overlap or charge transfer between the π-orbitals of the ring and the σ*(T-F) antibonding orbital might affect the magnitude of the T-F σ-hole. However, NBO analysis did not indicate any relevant interorbital transfers.

The total interaction energy can be divided into its various components by any of several partitioning schemes. The results of an EDA/BLYP-D3/ZORA/TZ2P decomposition are displayed in Table S2. As is immediately clear, the electrostatic term makes the largest contribution to these interactions, accounting for some 60-65% of the total attractive energy. The orbital interaction component, of which charge transfer is a part, makes up 30-40%, with only a very small contribution from dispersion, amounting to only 4% or so. These percentage contributions are fairly consistent across the entire spectrum of tetrel bonds, whether T-F or T-C, and regardless of the identity of the tetrel atom.

3.2.3 Comparison with Experimental Crystal Structures.

A survey of the CSD (Cambridge Structural Database)[96] provides several examples of crystal structures of complexes of the sort considered here. Table S3 provides pictorial versions of these examples with a central T atom covalently bonded to three halogens and a phenyl ring, plus another interaction with a nucleophile[100-105]. Several of these have the nucleophile opposite a halogen substituent, and another opposite the phenyl ring. They all have the essential shape of a trigonal bipyramid, as discussed here. Despite other forces within the crystal, the tetrel bond distances fall within the range of those computed here for analogous systems.

4. DISCUSSION

There is some precedent in the literature dealing with competition between multiple possible sites of tetrel bonding, coupled with large-scale deformation of the Lewis acid. When a tetrel atom is bonded to four F substituents, an incoming nucleophile will induce TF_4 to rearrange [106] into a trigonal bipyramidal shape. This structure contains a vacancy for the base at either an axial or equatorial site. The placement of the base in an equatorial site leads to a very high interaction energy, on the order of 50 kcal/mol. But in order to provide this equatorial site, the deformation of the TF_4 is much larger than what is needed for it to accommodate an axial nucleophile position. So although the axial location of the nucleophile is more weakly bonded to the tetrel atom, its smaller deformation energy makes this the preferred bonding site. This overall energetic preference is most dramatic for the smaller tetrel atoms which also suffer the highest degree of deformation energy [107]. Also consistent with the trends noted here, the deformation of TF_4 from a tetrahedral to a trigonal bipyramid shape intensifies the σ-hole by a great deal.

A related study[108] considered the feasibility of the TF_4 molecule engaging in two tetrel bonds simultaneously. In order to do so, TF_4 must undergo a geometrical transition to an octahedral structure so as to accommodate the four covalent bonds and two tetrel bonds. The two nucleophiles can occupy syn positions, with each of them in a σ-hole directly opposite a T-F bond. The alternative geometry places the two nucleophiles opposite one another in an anti configuration. As such they are each attracted by a π-hole above and below the plane of the D_{4h} TF_4 segment. Again, the deformation energies were found crucial to the relative stabilities of the two possibilities. The latter square TF_4 offers an unobstructed path of the bases to the π-holes and enjoy a large interaction energy. On the other hand, the energy required for the originally tetrahedral TF_4 to distort to the requisite square geometry is much larger than that needed to adopt the see-saw structure needed to form the syn trimer. And once again, the high deformation energy overwhelms the stronger intrinsic binding, and it is the syn structure that prevails. It was also found that the π-holes associated with the planar TF_4 unit are very much more intense than those in the normal tetrahedral structure, which adds to the binding energy.

These sorts of effects are not limited exclusively to tetrel bonds. A recent set of calculations [109] extended these ideas to pnicogen bonds as well. Two F atoms and a phenyl ring were covalently bonded to one of several pnicogen (Z) atoms, in a pyramidal ZF_2Ph Lewis acid. A base could therefore approach along a σ-hole opposite a Z-F bond, or toward a π-hole situated opposite the Z lone pair. Although the σ-holes are more intense than their π-hole counterparts, it is the latter which engages in stronger interactions with the base, with much larger interaction energies. However, the requisite deformation of the ZF_2Ph to accommodate the π-hole base is far larger than that needed for the σ-hole approach. And once again, the latter effect dominates the overall interaction, making the σ-hole complexes more stable overall. Large deformation energies are not limited to the standard covalency of these central atoms. Not only are they present in TF_4 but also [65, 110] in hypervalent pnicogen, chalcogen, and halogen bonds.

There is ample evidence in the literature to support some of the general trends observed here. For example, the idea that larger T atoms result in stronger tetrel bonds has been documented, along with a leveling off between Sn and Pb [107, 111-117]. The deformation of a tetrahedral TR_4 molecule into a trigonal bipyramid upon formation of a tetrel bond has also become well recognized [40, 118, 119]. The concept of a deformation causing a large change in electrostatic potential has also been observed in related systems, including pnicogen-centered Lewis acids [120].

Within the realm of competing sites, there has been some elucidation of tetrel bonds to σ vs π-holes. One work [117] considered this question in the context of different molecules for each type of hole: TR_4 vs $TR_2{=}CH_2$. The π-sites were found to engage in the stronger bonding, as was the case for the comparison of TFH_3 vs $R_2T{=}O$ [121], consistent with other work as well [113, 116, 118, 122], even though it is the σ-hole that predominates over π in aerogen bonds [123]. Other work has compared σ with π-holes in the context of two different sorts of bonds, as in for example a σ-hole tetrel with a π-hole pnicogen bond [124].

5. CONCLUSIONS

In summary, it has been shown here that the question as to which site offers the best opportunity to form a tetrel bond cannot be answered solely on the basis of the substituent which presents the most intense σ-hole. In the examples studied here, a position opposite the highly electron-withdrawing F atom induces a σ-hole in the monomer that is more intense than one opposite a phenyl ring, as one might expect. Nevertheless, a nucleophile engages in a stronger interaction in the latter position.

This apparent paradox is resolved when considering the change in geometry of the Lewis acid from tetrahedral to trigonal bipyramid within the context of the complex. While this distortion amplifies the σ-hole intensity in both site locations, there is a much larger increase in the hole opposite the phenyl group, reversing the order observed in the isolated monomer, and favoring the phenyl over the T-F site.

A second factor that must be considered is the energetic cost for the monomer to achieve the internal structure required to engage in a tetrel bond. This deformation energy is quite substantial amounting to more than 20 kcal/mol in some cases so can hardly be ignored, particularly for the smaller tetrel atoms which are burdened by the largest deformation energies. This quantity is consistently larger for the sites lying opposite the phenyl ring, due to the more stringent steric constraints associated with this larger substituent. The deformation thus tends to favor the T-F sites, a pattern opposite to the interaction energies between the pre-deformed monomers. These two conflicting trends lead to binding energies that are roughly comparable for the two sites. The T-F site is favored, albeit by only a small amount, for the smaller Si and Ge tetrel atoms, while the larger Pb prefers the T-C site; there is little distinction between the two sites for the intermediate-sized Sn.

With respect to the electron-withdrawing power of the phenyl group, trisubstitution by F or CH_3 groups have the expected effects upon the binding and interaction energies. The trifluoro-substituent is particularly potent, especially with regard to the T-C site opposite the ring,

amplifying these energetic measures by several kcal/mol. On the other hand, the electron-withdrawing capacity of the ring is unable to reverse the preference of a nucleophile for the T-F vs T-C site.

Conflicts of interest

There are no conflicts to declare.

Acknowledgements

This work was financed in part by a statutory activity subsidy from the Polish Ministry of Science and Higher Education for the Faculty of Chemistry of Wroclaw University of Science and Technology. A generous computer time from the Wroclaw Supercomputer and Networking Center is acknowledged.

References

1. G. R. Desiraju, *Journal of the American Chemical Society*, 2013, **135**, 9952-9967.
2. G. R. Desiraju and T. Steiner, *The weak hydrogen bond: in structural chemistry and biology*, International Union of Crystal, 2001.
3. H.-J. Schneider, *Angewandte Chemie International Edition*, 2009, **48**, 3924-3977.
4. H.-J. Schneider and A. K. Yatsimirsky, *Principles and methods in supramolecular chemistry*, J. Wiley, 2000.
5. J.-M. Lehn, *Science*, 2002, **295**, 2400.
6. S. I. Stupp, V. LeBonheur, K. Walker, L. S. Li, K. E. Huggins, M. Keser and A. Amstutz, *Science*, 1997, **276**, 384.
7. G. M. Whitesides, J. P. Mathias and C. T. Seto, *Science*, 1991, **254**, 1312.
8. P. Cordier, F. Tournilhac, C. Soulié-Ziakovic and L. Leibler, *Nature*, 2008, **451**, 977.
9. P. R. Varadwaj, A. Varadwaj, H. M. Marques and K. Yamashita, *Sci Rep-Uk*, 2019, **9**.
10. K. Kendall and A. D. Roberts, *Philosophical transactions of the Royal Society of London. Series B, Biological sciences*, 2015, **370**, 20140078-20140078.
11. J. Y. C. Lim and P. D. Beer, *Chem*, 2018, **4**, 731-783.
12. L. Strekowski and B. Wilson, *Mutation Research/Fundamental and Molecular Mechanisms of Mutagenesis*, 2007, **623**, 3-13.
13. S. Scheiner, *Molecules*, 2019, **24**, 227.
14. R. C. Trievel and S. Scheiner, *Molecules*, 2018, **23**.
15. S. Scheiner, *J Phys Chem A*, 2017, **121**, 3606-3615.
16. Y.-Z. Liu, K. Yuan, L. Liu, Z. Yuan and Y.-C. Zhu, *The Journal of Physical Chemistry A*, 2017, **121**, 892-900.
17. M. Zurro, S. Asmus, J. Bamberger, S. Beckendorf and O. García Mancheño, *Chemistry – A European Journal*, 2016, **22**, 3785-3793.
18. V. Amendola, G. Bergamaschi, M. Boiocchi, L. Legnani, E. L. Presti, A. Miljkovic, E. Monzani and F. Pancotti, *Chemical Communications*, 2016, **52**, 10910-10913.
19. J. S. Murray, P. Lane, T. Clark, K. E. Riley and P. Politzer, *Journal of Molecular Modeling*, 2012, **18**, 541-548.
20. J. S. Murray, P. Lane and P. Politzer, *Journal of Molecular Modeling*, 2009, **15**, 723-729.

21. P. Politzer, J. S. Murray and M. C. Concha, *Journal of Molecular Modeling*, 2008, **14**, 659-665.
22. J. S. Murray, P. Lane, T. Clark and P. Politzer, *Journal of Molecular Modeling*, 2007, **13**, 1033-1038.
23. T. Clark, M. Hennemann, J. S. Murray and P. Politzer, *Journal of Molecular Modeling*, 2007, **13**, 291-296.
24. P. Politzer, J. S. Murray and T. Clark, *Phys Chem Chem Phys*, 2013, **15**, 11178-11189.
25. P. Politzer and J. S. Murray, *Chemphyschem*, 2013, **14**, 278-294.
26. P. Politzer, K. E. Riley, F. A. Bulat and J. S. Murray, *Comput Theor Chem*, 2012, **998**, 2-8.
27. P. Politzer and J. S. Murray, *Theoretical Chemistry Accounts*, 2012, **131**.
28. P. Politzer, J. S. Murray and T. Clark, *Phys Chem Chem Phys*, 2010, **12**, 7748-7757.
29. P. Politzer, J. S. Murray and M. C. Concha, *Journal of Molecular Modeling*, 2007, **13**, 643-650.
30. P. Politzer, P. Lane, M. C. Concha, Y. G. Ma and J. S. Murray, *Journal of Molecular Modeling*, 2007, **13**, 305-311.
31. J. S. Murray, P. Lane and P. Politzer, *Int J Quantum Chem*, 2007, **107**, 2286-2292.
32. A. J. Stone, *Journal of the American Chemical Society*, 2013, **135**, 7005-7009.
33. A. P. Orlova and P. G. Jasien, *Comput Theor Chem*, 2018, **1139**, 63-69.
34. M. A. Ben Aissa, S. Hassen and Y. Arfaoui, *Int J Quantum Chem*, 2019, **119**.
35. D. J. Pascoe, K. B. Ling and S. L. Cockroft, *Journal of the American Chemical Society*, 2017, **139**, 15160-15167.
36. J. Y. Wu, H. Yan, A. G. Zhong, H. Chen, Y. X. Jin and G. L. Dai, *Journal of Molecular Modeling*, 2019, **25**.
37. L. Y. Guan and Y. R. Mo, *J Phys Chem A*, 2014, **118**, 8911-8921.
38. Y. Zhang, W. Z. Wang and Y. B. Wang, *Comput Theor Chem*, 2019, **1147**, 8-12.
39. M. D. Esrafili and P. Mousavian, *Molecules*, 2018, **23**.
40. M. D. Esrafili, S. Asadollahi and P. Mousavian, *Chem. Phys. Lett.*, 2018, **691**, 394-400.
41. A. Frontera and A. Bauza, *Phys Chem Chem Phys*, 2017, **19**, 30063-30068.
42. E. Makarewicz, J. Lundell, A. J. Gordon and S. Berski, *J Comput Chem*, 2016, **37**, 1876-1886.
43. A. Bauzá and A. Frontera, *Angewandte Chemie International Edition*, 2015, **54**, 7340-7343.
44. A. Bauza and A. Frontera, *Chemphyschem*, 2015, **16**, 3625-3630.
45. J. S. Murray and P. Politzer, *Wiley Interdisciplinary Reviews-Computational Molecular Science*, 2011, **1**, 153-163.
46. P. Politzer and J. S. Murray, *Journal of Computational Chemistry*, 2018, **39**, 464-471.
47. P. Politzer, J. S. Murray, T. Clark and G. Resnati, *Phys Chem Chem Phys*, 2017, **19**, 32166-32178.
48. P. Politzer and J. S. Murray, *Crystals*, 2017, **7**.
49. C. B. Aakeroy, S. Alavi, L. Brammer, D. L. Bryce, T. Clark, J. E. Del Bene, A. J. Edwards, C. Esterhuysen, T. N. G. Row, P. Kennepohl, A. C. Legon, G. O. Lloyd, J. S. Murray, W. T. Pennington, P. Politzer, K. E. Riley, S. V. Rosokha, S. Scheiner, S. Tsuzuki and I. Vargas-Baca, *Faraday Discussions*, 2017, **203**, 131-163.
50. M. Hennemann, J. S. Murray, P. Politzer, K. E. Riley and T. Clark, *Journal of Molecular Modeling*, 2012, **18**, 2461-2469.

51. J. S. Murray and P. Politzer, *Wiley Interdisciplinary Reviews-Computational Molecular Science*, 2017, **7**.
52. M. D. Esrafili, P. Mousavian and F. Mohammadian-Sabet, *Molecular Physics*, 2019, **117**, 58-66.
53. M. Bortoli, S. M. Ahmad, T. A. Hamlin, F. M. Bickelhaupt and L. Orian, *Phys Chem Chem Phys*, 2018, **20**, 27592-27599.
54. M. D. Esrafili and F. Mohammadian-Sabet, *Structural Chemistry*, 2016, **27**, 617-625.
55. M. D. Esrafili and N. Mohammadirad, *Journal of Molecular Modeling*, 2015, **21**.
56. K. E. Riley, J. S. Murray, J. Fanfrlik, J. Rezac, R. J. Sola, M. C. Concha, F. M. Ramos and P. Politzer, *Journal of Molecular Modeling*, 2013, **19**, 4651-4659.
57. K. E. Riley, J. S. Murray, J. Fanfrlik, J. Rezac, R. J. Sola, M. C. Concha, F. M. Ramos and P. Politzer, *Journal of Molecular Modeling*, 2011, **17**, 3309-3318.
58. K. E. Riley and P. Hobza, *Phys Chem Chem Phys*, 2013, **15**, 17742-17751.
59. I. Alkorta, J. Elguero and J. E. Del Bene, *J Phys Chem A*, 2013, **117**, 10497-10503.
60. V. Oliveira, E. Kraka and D. Cremer, *Phys Chem Chem Phys*, 2016, **18**, 33031-33046.
61. V. Vasylyeva, L. Catalano, C. Nervi, R. Gobetto, P. Metrangolo and G. Resnati, *CrystEngComm*, 2016, **18**, 2247-2250.
62. J. Řezáč and A. de la Lande, *Phys Chem Chem Phys*, 2017, **19**, 791-803.
63. M. D. Esrafili and A. Sadr-Mousavi, *Journal of Molecular Graphics & Modelling*, 2017, **75**, 165-173.
64. U. Adhikari and S. Scheiner, *Chemical Physics Letters*, 2012, **532**, 31-35.
65. W. Zierkiewicz, M. Michalczyk and S. Scheiner, *Phys Chem Chem Phys*, 2018, **20**, 8832-8841.
66. W. Zierkiewicz, M. Michalczyk and S. Scheiner, *Phys Chem Chem Phys*, 2018, **20**, 22498-22509.
67. W. Zierkiewicz, M. Michalczyk, D. Bienko, D. Michalska and T. Zeegers-Huyskens, *Int J Quantum Chem*, 2017, **117**.
68. W. Zierkiewicz and M. Michalczyk, *Theoretical Chemistry Accounts*, 2017, **136**.
69. J. Fanfrlik, W. Zierkiewicz, P. Svec, Z. Ruzickova, J. Rezac, M. Michalczyk, A. Ruzicka, D. Michalska and P. Hobza, *Journal of Molecular Modeling*, 2017, **23**.
70. A. Bauzá, T. J. Mooibroek and A. Frontera, *Angewandte Chemie International Edition*, 2013, **52**, 12317-12321.
71. H. Xu, J. Cheng, X. Yu and Q. Li, *ChemistrySelect*, 2018, **3**, 2842-2849.
72. Y. X. Wei and Q. Z. Li, *Molecular Physics*, 2018, **116**, 222-230.
73. S. J. Grabowski, *Molecules*, 2018, **23**.
74. W. B. Dong, X. Yang, J. B. Cheng, W. Z. Li and Q. Z. Li, *Journal of Fluorine Chemistry*, 2018, **207**, 38-44.
75. S. Scheiner, *J Phys Chem A*, 2017, **121**, 5561-5568.
76. C. Trujillo, I. Alkorta, J. Elguero and G. Sanchez-Sanz, *Molecules*, 2019, **24**.
77. J. A. Kelly, M. Juckel, T. J. Hadlington, I. Fernandez, G. Frenking and C. Jones, *Chem-Eur J*, 2019, **25**, 2773-2785.
78. S. P. Gnanasekar and E. Arunan, *J Phys Chem A*, 2019, **123**, 1168-1176.
79. A. Bauza, S. K. Seth and A. Frontera, *Coordin Chem Rev*, 2019, **384**, 107-125.
80. A. Frontera and A. Bauzá, *Chemistry – A European Journal*, 2018, **24**, 16582-16587.
81. T. H. Dunning, *Journal of Chemical Physics*, 1989, **90**, 1007-1023.
82. C. Moller and M. S. Plesset, *Physical Review*, 1934, **46**, 0618-0622.

83. K. A. Peterson, *Journal of Chemical Physics*, 2003, **119**, 11099-11112.
84. A. D. Becke, *Journal of Chemical Physics*, 1993, **98**, 5648-5652.
85. C. T. Lee, W. T. Yang and R. G. Parr, *Physical Review B*, 1988, **37**, 785-789.
86. K. Raghavachari, G. W. Trucks, J. A. Pople and M. Headgordon, *Chemical Physics Letters*, 1989, **157**, 479-483.
87. S. F. Boys and F. Bernardi, *Molecular Physics*, 1970, **19**, 553-&.
88. T. Lu and F. Chen, 2012, **33**, 580-592.
89. T. Lu and F. Chen, *Journal of Molecular Graphics and Modelling*, 2012, **38**, 314-323.
90. F. A. Bulat, A. Toro-Labbe, T. Brinck, J. S. Murray and P. Politzer, *Journal of Molecular Modeling*, 2010, **16**, 1679-1691.
91. A. T. Keith, *Journal*, 2014.
92. E. D. Glendening, C. R. Landis and F. Weinhold, *Journal of Computational Chemistry*, 2013, **34**, 1429-1437.
93. *Journal*, 2014.
94. C. F. Guerra, J. G. Snijders, G. te Velde and E. J. Baerends, *Theoretical Chemistry Accounts*, 1998, **99**, 391-403.
95. G. te Velde, F. M. Bickelhaupt, E. J. Baerends, C. F. Guerra, S. J. A. Van Gisbergen, J. G. Snijders and T. Ziegler, *Journal of Computational Chemistry*, 2001, **22**, 931-967.
96. C. R. Groom, I. J. Bruno, M. P. Lightfoot and S. C. Ward, *Acta Crystallographica Section B-Structural Science Crystal Engineering and Materials*, 2016, **72**, 171-179.
97. M. J. Frisch, Trucks, G. W. ; Schlegel, H. B.; Scuseria, G. E.; Robb, M. A.; Cheeseman, J. R.; Scalmani, G.; Barone, V.; Mennucci, B.; Petersson, G. A.; Nakatsuji, H.; Caricato, M.; Li, X.; Hratchian, H. P.; Izmaylov, A. F.; Bloino, J.; Zheng, G.; Sonnenberg, J. L.; Hada, M.; Ehara, M.; Toyota, K.; Fukuda, R.; Hasegawa, J.; Ishida, M.; Nakajima, T.; Honda, Y.; Kitao, O.; Nakai, H.; Vreven, T.; Montgomery, J. A., Jr.; Peralta, J. E.; Ogliaro, F.; Bearpark, M.; Heyd, J. J.; Brothers, E.; Kudin, K. N.; Staroverov, V. N.; Kobayashi, R.; Normand, J.; Raghavachari, K.; Rendell, A.; Burant, J. C.; Iyengar, S. S.; Tomasi, J.; Cossi, M.; Rega, N.; Millam, J. M.; Klene, M.; Knox, J. E.; Cross, J. B.; Bakken, V.; Adamo, C.; Jaramillo, J.; Gomperts, R.; Stratmann, R. E.; Yazyev, O.; Austin, A. J.; Cammi, R.; Pomelli, C.; Ochterski, J. W.; Martin, R. L.; Morokuma, K.; Zakrzewski, V. G.; Voth, G. A.; Salvador, P.; Dannenberg, J. J.; Dapprich, S.; Daniels, A. D.; Farkas, Ö.; Foresman, J. B.; Ortiz, J. V.; Cioslowski, J.; Fox, *Journal*, 2009, **E.01**.
98. R. F. W. Bader, *J Phys Chem A*, 1998, **102**, 7314-7323.
99. R. F. W. Bader and H. Essen, *Journal of Chemical Physics*, 1984, **80**, 1943-1960.
100. Y. Tokoro, H. Yeo, K. Tanaka and Y. Chujo, *Chemical Communications*, 2012, **48**, 8541-8543.
101. W. Clegg, *CSD Communication(Private Communication)*, 2016.
102. W. Clegg, C. M. J. Grievson and K. Wade, *J Chem Soc Chem Comm*, 1987, **13**, 969-970.
103. N. Kano, F. Komatsu, M. Yamamura and T. Kawashima, *Journal of the American Chemical Society*, 2006, **128**, 7097-7109.
104. T. Leonhardt and H. P. Latscha, *Z Naturforsch B*, 1997, **52**, 25-29.
105. J. S. Casas, E. E. Castellano, F. J. G. Barros, A. Sanchez, A. S. Gonzalez, J. Sordo and J. ZukermanSchpector, *J Organomet Chem*, 1996, **519**, 209-216.
106. W. Zierkiewicz, M. Michalczyk, R. Wysokiński and S. Scheiner, *Molecules*, 2019, **24**, 376.
107. S. Scheiner, *J. Phys. Chem. A*, 2018, **122**, 2550-2562.

108. M. Michalczyk, W. Zierkiewicz, R. Wysokinski and S. Scheiner, *Chemphyschem*, 2019 **(in press)**.
109. W. Zierkiewicz, M. Michalczyk, R. Wysokinski and S. Scheiner, *Journal of Molecular Modeling*, 2019 **(in press)**.
110. S. Scheiner and J. Lu, *Chem. Eur. J.*, 2018, **24**, 8167-8177.
111. K. J. Donald and M. Tawfik, *J Phys Chem A*, 2013, **117**, 14176-14183.
112. S. Scheiner, *J. Phys. Chem. A*, 2017, **121**, 5561-5568.
113. Y. Wei and Q. Li, *Molecular Physics*, 2018, **116**, 222-230.
114. Y.-X. Wei, H.-B. Li, J.-B. Cheng, W.-Z. Li and Q.-Z. Li, *Int J Quantum Chem*, 2017, **117**, e25448.
115. M. Liu, Q. Li, W. Li and J. Cheng, *Structural Chemistry*, 2017, **28**, 823-831.
116. W. Dong, B. Niu, S. Liu, J. Cheng, S. Liu and Q. Li, *ChemPhysChem*, 2019, **20**, 627-635.
117. W. Zierkiewicz, M. Michalczyk and S. Scheiner, *Molecules*, 2018, **23**, 1416.
118. S. J. Grabowski, *Phys Chem Chem Phys*, 2017, **19**, 29742-29759.
119. S. J. Grabowski and W. A. Sokalski, *ChemPhysChem*, 2017, **18**, 1569-1577.
120. J. Fanfrlík, W. Zierkiewicz, P. Švec, Z. Růžičková, J. Řezáč, M. Michalczyk, A. Růžička, D. Michalska and P. Hobza, *Journal of Molecular Modeling*, 2017, **23**, 328.
121. J. Zhang, Q. Hu, Q. Li, S. Scheiner and S. Liu, *Int J Quantum Chem*, 2019, **119(11)**, e25910.
122. H. Xu, J. Cheng, X. Yang, Z. Liu, W. Li and Q. Li, *ChemPhysChem*, 2017, **18**, 2442-2450.
123. W. Zierkiewicz, M. Michalczyk and S. Scheiner, *Phys Chem Chem Phys*, 2018, **20**, 4676-4687.
124. W. Dong, Y. Wang, J. Cheng, X. Yang and Q. Li, *Molecular Physics*, 2019, **117**, 251-259.

Table 1. Molecular electrostatic potential maxima (in kcal/mol) on the 0.001 a.u. surface of the electron density ($V_{s,max}$) of $TF_3C_6H_2R_3$ monomers calculated at the MP2/aug-cc-pVDZ level of theory.

Isolated molecule	$V_{S,max}$ (T-F) σ-hole	$V_{S,max}$ (T-C) σ-hole
$CF_3C_6H_5$	8.6	1.4
$CF_3C_6H_2F_3$	17.8	9.9
$CF_3C_6H_2(CH_3)_3$	5.0	-2.1
$SiF_3C_6H_5$	31.8	25.4
$SiF_3C_6H_2F_3$	42.0	35.1
$SiF_3C_6H_2(CH_3)_3$	27.4	21.0
$GeF_3C_6H_5$	38.3	23.4
$GeF_3C_6H_2F_3$	46.3	32.0
$GeF_3C_6H_2(CH_3)_3$	33.6	19.0
$SnF_3C_6H_5$	54.3	33.2
$SnF_3C_6H_2F_3$	64.9	44.3
$SnF_3C_6H_2(CH_3)_3$	46.6	28.3
$PbF_3C_6H_5$	53.7	18.5
$PbF_3C_6H_2F_3$	64.5	29.0
$PbF_3C_6H_2(CH_3)_3$	49.1	13.3

Table 2. Difference (kcal/mol) in electronic and Gibbs free energy at 25 C (in parentheses) between T-F vs T-C complex of indicated molecules with NH_3, calculated at the MP2/aug-cc-pVDZ (I), and BLYP-D3/aug-cc-pVDZ (II), levels of theory.

	(I)	(II)
$SiF_3C_6H_5$	2.14 (2.56)	1.45 (1.84)
$SiF_3C_6H_2F_3$	0.18 (0.56)	-0.32 (0.10)
$SiF_3C_6H_2(CH_3)_3$	2.78 (2.86)	2.03 (2.55)
$GeF_3C_6H_5$	0.64 (0.52)	0.14 (-0.17)
$GeF_3C_6H_2F_3$	-0.88 (-1.40)	-1.23 (-1.07)
$GeF_3C_6H_2(CH_3)_3$	1.31 (0.87)	0.72 (1.14)
$SnF_3C_6H_5$	-0.71 (-1.49)	-1.99 (-1.87)
$SnF_3C_6H_2F_3$	-1.60 (-3.00)	-2.73 (-2.60)
$SnF_3C_6H_2(CH_3)_3$	-0.12 (-1.05)	-1.45 (-1.18)
$PbF_3C_6H_5$	-3.71 (-2.92)	-3.55 (-3.32)
$PbF_3C_6H_2F_3$	-4.32 (-3.76)	-4.11 (-3.25)
$PbF_3C_6H_2(CH_3)_3$	-3.42 (-2.26)	-3.27 (-2.79)

[a] Gibbs free energies are given in parenthesis.

Table 3. Binding energies (E_b, kcal/mol) of $TF_3C_6H_2R_3$ complexes with NH_3 calculated at the MP2/aug-cc-pVDZ (I), BLYP-D3/ aug-cc-pVDZ (II) and CCSD(T)/aug-cc-pVDZ (III) levels of theory.

	(T-F) σ-hole			(T-C) σ-hole		
	(I)	(II)	(III)	(I)	(II)	(III)
$SiF_3C_6H_5$	-4.45	-3.94	-3.73	-2.14	-2.19	-1.63
$SiF_3C_6H_2F_3$	-5.64	-5.57	-5.15	-5.29	-5.20	-5.02
$SiF_3C_6H_2(CH_3)_3$	-3.94	-3.29	-3.37	-0.90	-1.00	-0.56
$GeF_3C_6H_5$	-8.22	-7.87	-7.67	-6.33	-7.51	-5.67
$GeF_3C_6H_2F_3$	-9.69	-9.32	-9.30	-9.42	-10.33	-8.95
$GeF_3C_6H_2(CH_3)_3$	-7.75	-7.18	-7.32	-5.11	-6.19	-4.60
$SnF_3C_6H_5$	-17.02	-15.01	-16.79	-17.77	-17.42	-17.43
$SnF_3C_6H_2F_3$	-18.87	-16.90	-18.71	-20.40	-20.01	-20.22
$SnF_3C_6H_2(CH_3)_3$	-16.43	-14.50	-16.27	-16.46	-16.29	-16.25
$PbF_3C_6H_5$	-15.11	-14.45	-14.78	-17.66	-18.16	-16.85
$PbF_3C_6H_2F_3$	-16.71	-16.30	-16.41	-20.11	-20.47	-19.45
$PbF_3C_6H_2(CH_3)_3$	-14.29	-13.69	-14.02	-16.68	-17.10	-15.97

Table 4. Structural parameters (distances in Å, angles in degrees) in $TF_3C_6H_2R_3$ (T = Si, Ge, Sn, Pb; R = H, F, CH_3) complexes with ammonia calculated at the MP2/aug-cc-pVDZ level of theory.

	(T-F) σ-hole				(T–C) σ-hole		
	R(T···N)	θ(F-T···N)	Φ(C-C-T···N)	Σθ(F-T-F) (Δ)[a]	R(T···N)	θ(C-T···N)	Σθ(F-T-F) (Δ)[a]
$SiF_3C_6H_5$	2.168	173.4	62.5	310.0 (-10.7)	2.089	179.6	352.9 (32.2)
$SiF_3C_6H_2F_3$	2.152	173.6	61.6	311.4 (-11.2)	2.069	179.4	354.0 (31.4)
$SiF_3C_6H_2(CH_3)_3$	2.170	173.0	58.8	309.2 (-10.6)	2.097	179.4	352.5 (32.7)
$GeF_3C_6H_5$	2.221	169.2	35.3	304.6 (-11.8)	2.117	179.0	351.5 (35.1)
$GeF_3C_6H_2F_3$	2.205	169.2	25.1	305.4 (-13.3)	2.104	178.7	352.6 (33.9)
$GeF_3C_6H_2(CH_3)_3$	2.222	168.6	30.4	303.3 (12.0)	2.121	178.8	351.2 (35.9)
$SnF_3C_6H_5$	2.346	167.1	0.0	301.4 (-11.3)	2.246	174.0	349.2 (36.5)
$SnF_3C_6H_2F_3$	2.337	168.6	0.0	303.5 (-12.0)	2.235	173.2	349.9 (34.4)
$SnF_3C_6H_2(CH_3)_3$	2.350	166.8	0.0	300.5 (-11.0)	2.245	173.6	347.8 (36.3)
$PbF_3C_6H_5$	2.501	164.2	0.0	293.6 (-11.1)	2.278	171.1	346.0 (41.3)
$PbF_3C_6H_2F_3$	2.479	167.6	0.0	296.8 (-10.8)	2.275	170.8	347.6 (40.0)
$PbF_3C_6H_2(CH_3)_3$	2.501	165.4	1.2	293.6 (-10.0)	2.279	171.7	345.4 (41.8)

[a]change from optimized monomer.

Table 5. Deformation energies (E_{def}, kcal/mol) of $TF_3C_6H_2R_3$ complexes with NH_3 calculated at the MP2/aug-cc-pVDZ level of theory.

	(T-F) σ-hole			
	$E_{def}(TF_3C_6H_2R_3)$	$E_{def}(NH_3)$	E_{def}	$V_{S,max}$ (Δ)
$SiF_3C_6H_5$	14.08	0.06	14.14	65.1 (+33.2)
$SiF_3C_6H_2F_3$	15.24	0.05	15.29	75.9 (+33.9)
$SiF_3C_6H_2(CH_3)_3$	13.89	0.06	13.95	60.4 (+33.0)
$GeF_3C_6H_5$	12.09	0.11	12.20	71.1 (+32.8)
$GeF_3C_6H_2F_3$	13.22	0.10	13.32	83.6 (+37.3)
$GeF_3C_6H_2(CH_3)_3$	11.95	0.11	12.06	66.8 (+33.2)
$SnF_3C_6H_5$	6.94	0.10	7.04	76.8 (+22.5)
$SnF_3C_6H_2F_3$	7.27	0.10	7.28	87.8 (+22.9)
$SnF_3C_6H_2(CH_3)_3$	6.74	0.11	6.84	72.2 (+25.5)
$PbF_3C_6H_5$	3.34	0.13	3.47	65.1 (+11.3)
$PbF_3C_6H_2F_3$	3.17	0.09	3.26	75.5 (+10.9)
$PbF_3C_6H_2(CH_3)_3$	2.81	0.10	2.91	59.9 (+10.8)
	(T-C) σ-hole			
$SiF_3C_6H_5$	22.72	0.09	22.81	83.3 (+57.9)
$SiF_3C_6H_2F_3$	23.12	0.08	23.20	93.9 (+58.8)
$SiF_3C_6H_2(CH_3)_3$	22.72	0.09	22.81	79.6 (+68.6)
$GeF_3C_6H_5$	20.45	0.16	20.61	80.3 (+56.9)
$GeF_3C_6H_2F_3$	20.43	0.15	20.47	90.4 (+58.4)
$GeF_3C_6H_2(CH_3)_3$	20.63	0.16	20.79	76.8 (+75.1)
$SnF_3C_6H_5$	14.47	0.31	14.78	86.9 (+53.8)
$SnF_3C_6H_2F_3$	13.29	0.14	13.44	95.4 (+51.2)
$SnF_3C_6H_2(CH_3)_3$	13.81	0.16	13.97	81.8 (+53.5)
$PbF_3C_6H_5$	12.46	0.68	13.12	65.5 (+47.1)
$PbF_3C_6H_2F_3$	12.05	0.63	12.68	74.8 (+18.8)
$PbF_3C_6H_2(CH_3)_3$	12.66	0.70	13.36	61.3 (+48.0)

Table 6. Interaction energies (E_{int}, kcal/mol) of $TF_3C_6H_2R_3$ complexes with NH_3 calculated at the MP2/aug-cc-pVDZ (I), BLYP-D3/aug-cc-pVDZ (II), and CCSD(T)/aug-cc-pVDZ (III) levels of theory.

	(T-F) σ-hole			(T-C) σ-hole		
	(I)	(II)	(III)	(I)	(II)	(III)
$SiF_3C_6H_5$	-18.59	-14.67	-17.79	-24.94	-21.26	-24.93
$SiF_3C_6H_2F_3$	-20.93	-17.28	-20.35	-28.50	-25.16	-28.53
$SiF_3C_6H_2(CH_3)_3$	-17.89	-13.59	-17.23	-23.71	-19.70	-23.76
$GeF_3C_6H_5$	-20.42	-16.81	-19.72	-26.94	-23.89	-26.73
$GeF_3C_6H_2F_3$	-23.01	-19.17	-22.45	-29.88	-26.82	-29.69
$GeF_3C_6H_2(CH_3)_3$	-19.81	-15.69	-19.22	-25.91	-22.71	-25.77
$SnF_3C_6H_5$	-24.06	-20.29	-23.67	-32.55	-28.79	-32.44
$SnF_3C_6H_2F_3$	-26.24	-22.56	-25.92	-33.84	-30.99	-33.74
$SnF_3C_6H_2(CH_3)_3$	-23.28	-19.55	-22.97	-30.43	-27.84	-30.38
$PbF_3C_6H_5$	-18.58	-16.79	-18.16	-30.79	-26.34	-30.14
$PbF_3C_6H_2F_3$	-19.97	-18.91	-19.58	-32.79	-28.22	-32.14
$PbF_3C_6H_2(CH_3)_3$	-17.20	-15.86	-16.84	-30.05	-25.37	-29.48

Table 7. AIM bond critical point (BCP) properties: electron density ρ, Laplacian of electron density $\nabla^2\rho$ and total electron energy density (H) of tetrel bonded complexes with ammonia obtained at the MP2/aug-cc-pVDZ level. Data in atomic units.

	(T-F) σ-hole			(T-C) σ-hole		
	ρ	$\nabla^2\rho$	H	ρ	$\nabla^2\rho$	H
$SiF_3C_6H_5$	0.050	0.111	-0.018	0.057	0.185	-0.017
$SiF_3C_6H_2F_3$	0.051	0.125	-0.018	0.059	0.201	-0.017
$SiF_3C_6H_2(CH_3)_3$	0.049	0.110	-0.018	0.056	0.179	-0.017
$GeF_3C_6H_5$	0.058	0.138	-0.017	0.073	0.183	-0.024
$GeF_3C_6H_2F_3$	0.060	0.143	-0.018	0.075	0.191	-0.025
$GeF_3C_6H_2(CH_3)_3$	0.058	0.137	-0.016	0.072	0.182	-0.024
$SnF_3C_6H_5$	0.057	0.167	-0.009	0.072	0.218	-0.016
$SnF_3C_6H_2F_3$	0.058	0.171	-0.009	0.073	0.227	-0.016
$SnF_3C_6H_2(CH_3)_3$	0.056	0.166	-0.009	0.072	0.222	-0.015
$PbF_3C_6H_5$	0.049	0.135	-0.005	0.080	0.219	-0.018
$PbF_3C_6H_2F_3$	0.051	0.144	-0.006	0.080	0.220	-0.019
$PbF_3C_6H_2(CH_3)_3$	0.049	0.137	-0.005	0.079	0.219	-0.018

Table 8. NBO values of sum of the E(2) for NH_3 LP(N) donation (kcal/mol) to Lewis acid orbitals and total charge transfer (CT, me) from NH_3 to acid obtained at the BLYP-D3/aug-cc-pVDZ level.

	(T-F) σ-hole			(T-C) σ-hole		
	LP(N)→LV*(T)	LP(N)→σ*(T-C)	CT	LP(N)→LV*(T)	LP(N)→σ*(T-C)	CT
$SiF_3C_6H_5$	50.8	7.0	143	113.9	1.3	170
$SiF_3C_6H_2F_3$	55.6	7.8	153	122.8	1.4	181
$SiF_3C_6H_2(CH_3)_3$	49.2	6.6	139	109.8	1.2	165
$GeF_3C_6H_5$	43.5	7.9	151	98.7	0	200
$GeF_3C_6H_2F_3$	46.2	8.7	160	104.2	0	209
$GeF_3C_6H_2(CH_3)_3$	41.9	7.5	147	96.4	0	197
$SnF_3C_6H_5$	35.9	8.5	151	60.0	1.9	208
$SnF_3C_6H_2F_3$	37.8	10.0	160	62.3	1.8	215
$SnF_3C_6H_2(CH_3)_3$	35.2	8.1	148	56.7	2.0	205
$PbF_3C_6H_5$	20.9	6.2	121	35.5	4.5	226
$PbF_3C_6H_2F_3$	22.8	6.9	135	35.9	4.2	233
$PbF_3C_6H_2(CH_3)_3$	20.2	5.6	116	32.5	4.6	222

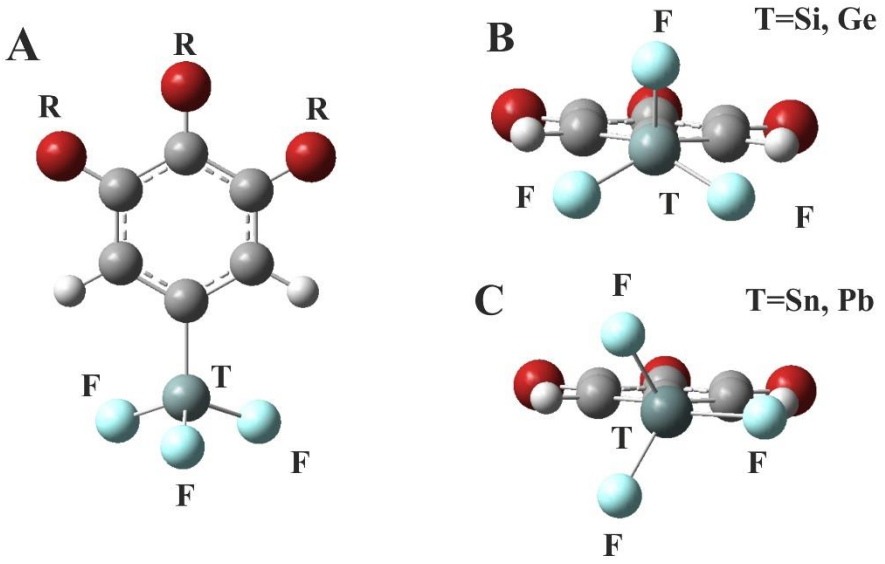

Fig. 1. Structures (A - top and B, C - side views) of optimized $TF_3C_6H_2R_3$ (T = Si, Ge, Sn, Pb; R = H, F, CH_3) monomers.

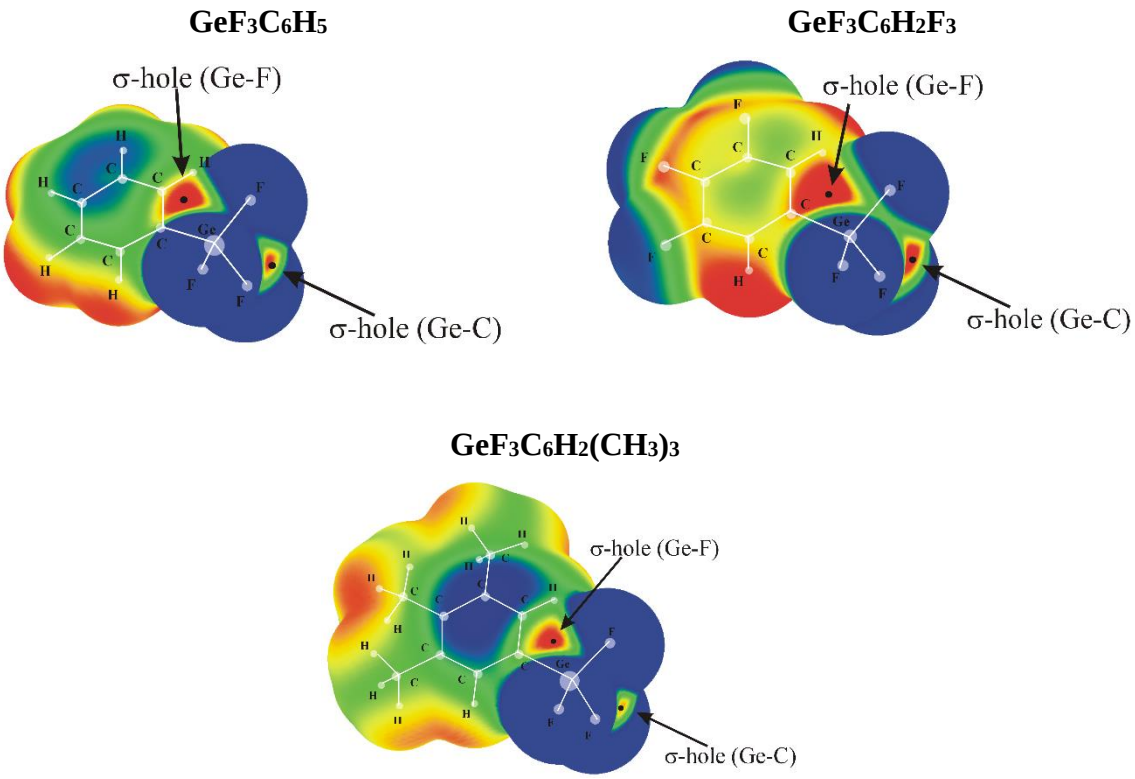

Fig. 2. MEPs of isolated Ge-containing molecules, computed on the 0.001 au isodensity surface at the MP2/aug-cc-pVDZ level. Colour ranges, in kcal/mol, are: red greater than 20, yellow between 10 and 20, green between 0 and 10, blue below 0 kcal/mol.

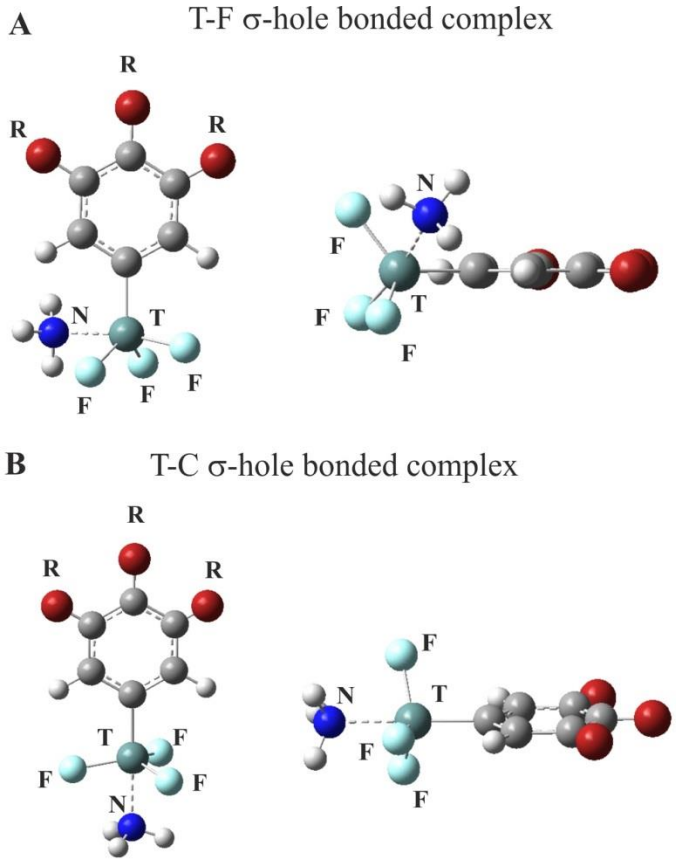

Fig. 3. MP2/aug-cc-pVDZ optimized structures (top and side views) of complexes of NH_3 with $TF_3C_6H_2R_3$ (T = Si, Ge, Sn, Pb; R = H, F, CH_3).